A High Resolution Scheme for Cavitating Flow

B. R. Shin[1*], S. J. Oh[1] and S. Obayashi[2]
1. Department of Mechanical Engineering, Changwon National University, Changwon 641-773, Korea, brshin@changwon.ac.kr
2. Institute of Fluid Science, Tohoku University, Sendai 980-8577, Japan

Abstract

A high resolution scheme for solving gas-liquid two-phase flows with cavitation is described. This scheme uses the curvilinear coordinate grid and solves the density based momentum equations for mixture of gas-liquid medium with a preconditioning method to treat both compressible and incompressible flow characteristics. The present preconditioned method is based on the Runge-Kutta explicit finite-difference scheme, and is improved by using the diagonalization, the flux difference splitting and the MUSCL-TVD schemes to save computational effort and to increase stability and resolvability, especially at gas-liquid contact surfaces. A homogeneous equilibrium cavitation model is used to treat the gas-liquid two-phase medium in cavitating flow as a locally homogeneous pseudo-single-phase medium. Therefore, it is easy to solve cavitating flow, including wave propagation, large density changes and incompressible flow characteristic at low Mach number. Some numerical results obtained by the present scheme are shown.

Keyword : Gsa-Liquid Two-Phase Flow, Cavitation, Preconditioning Method, TVD Scheme, Homogeneous Model,

1. Introduction

It is highly desired that high-speed hydraulic machinery and their equipments should have the confident operation, the wide operating range and the improved performance characteristics. In the estimation of the performance, the existence of unsteady cavity flow becomes a very important factor. Cavitation is a phase change phenomenon accompanying the appearance of vapor bubbles inside a homogeneous liquid medium that occurs in the domain below vapor pressure according to the decrease in local pressure when fluid devices move at high speed in a working fluid in the liquid state. Cavitation takes various forms according to the flow conditions, and causes noise, vibration and damage, as well as reduced performance in hydraulic machine systems when cavitation bubbles unexpectedly attach and collapse on body surfaces.

In order to reduce these unfavorable effects, technology for accurate prediction of cavitation is very important and becomes a common subject of study for designers of high-speed fluid devices. In recent years, fortunately, with the progression of computational environment largescale computations have become possible, and improvements in the prediction using numerical simulations are expected. However, because originally the cavity flows have strong unsteady flow phenomena including phase changes, fluid transients, vortex shedding and turbulence, the mathematical expression of cavity flow as well as the numerical method is expected to be very complex. Up to date, some efforts to propose cavity flow model and analytical method have been made. Among them, gas-liquid two-phase flow approaches with a concept of the homogeneous equilibrium [1-4] are more advantageous. Recently, we have proposed a mathematical cavity flow model [5,6] based on a homogeneous equilibrium model taking into account the compressibility of the gas-liquid two-phase media. With this model and TVD-MacCormack scheme [7] or a high-order MUSCL-TVD solution method [8], the mechanism of developing cavitation has been investigated through application to cavitating flows around a hydrofoil [9-12]. These schemes [9] were extended to preconditioned dual time-stepping methods [13,14] to treat both compressibility and incompressibility effects associated with very large range of mixture sound

speeds, which can arise in cavity flows with multi-rates of void fraction. In this paper we show a high resolution scheme for solving cavitating flow with some numerical examples.

2. Homogeneous Cavitation Model

The equation of state for the liquid phase can be expressed by Tammannn [15] as:

$$p_\ell + p_c = \rho_\ell K(T_\ell + T_c) \tag{1}$$

where p_ℓ, ρ_ℓ and T_ℓ are pressure, density, and temperature of the liquid (the subscript ℓ representing the liquid phase), K, p_c and T_c are the liquid constant, pressure and temperature constants of liquid. When the gas phase is assumed to be an ideal gas, the equation of state is

$$p_g = \rho_g R T_g \tag{2}$$

where R is the gas constant and the subscript g represents the gas phase.

In the locally homogeneous model of this study, the gas-liquid two-phase medium in the cavitating flow is treated as a locally homogeneous pseudo-single-phase medium. In the local volumetric element in gas-liquid two-phase medium, by supposing a limiting case of the bubble radius being infinitely small and the number of bubbles being infinitely large with the local α value being kept constant, a locally homogeneous medium can be obtained. By distributing the infinite number of infinitesimal bubbles in each computational cell having a different local void fraction, the gas-liquid mixture condition is specified macroscopically. Applying this model to the mixture condition inside the cavity, unsteady and complex cavity flows can be simulated.

The mixture density ρ of a two-phase medium is expressed by combining linearly a gas phase density ρ_g and a liquid phase density ρ_ℓ with the local void fraction α,

$$\rho = (1-\alpha)\rho_\ell + \alpha\rho_g \tag{3}$$

Then, assuming the local equilibrium conditions, the equation of state becomes, from Eqs.(1), (2) and (3),

$$\rho = (1-\alpha)\frac{p(p+p_c)}{K(T+T_c)} + \alpha\frac{p}{RT} \tag{4}$$

Also, between the local void fraction α and the quality (mass fraction of the gas phase) Y the following relation is obtained:

$$\rho(1-Y) = (1-\alpha)\rho_\ell, \quad \rho Y = \alpha\rho_g \tag{5}$$

Using Y from Eq.(5), the equation of state for a locally homogeneous compressible gas-liquid two-phase medium can be expressed as

$$\rho = \frac{p(p+p_c)}{K(1-Y)p(T+T_c) + RY(p+p_c)T} \tag{6}$$

where, p and T are the mixture pressure and the temperature. Therefore, the apparent compressibility is considered, and the sound speed c becomes

$$\begin{aligned} c^2 &= \rho C_p\left(\frac{\partial\rho}{\partial T} + \rho C_p\frac{\partial\rho}{\partial p}\right)^{-1} \\ &= \frac{C_p(p+p_c)^2 p}{\rho\{(p+p_c)^2(C_p - YR) - C_p(1-Y)\rho K(T+T_c)p_c - (1-Y)Kp(p+p_c)\}} \end{aligned} \tag{7}$$

C_p is the specific heat capacity at constant pressure of $C_p = YC_{pg} + (1-Y)C_{p\ell}$. And, the relation between the local void fraction α and the quality Y is given as

$$\alpha = \frac{RY(p+p_c)T}{K(1-Y)p(T+T_c) + RY(p+p_c)T} \tag{8}$$

It was confirmed that speed of sound predicted by Eq.(7) is well compared with Karplus' experimental data [16].

3. Fundamental Equations

Based on the cavitation model concept described in the Section 2 and neglecting the surface tension, the 2-D governing equations for the mixture mass, momentum, energy and the gas-phase mass conservation can be written in the curvilinear coordinates (ξ, η) as follows:

$$\frac{\partial \boldsymbol{Q}}{\partial t} + \frac{\partial \boldsymbol{E}}{\partial \xi} + \frac{\partial \boldsymbol{F}}{\partial \eta} = \frac{\partial \boldsymbol{E}_v}{\partial \xi} + \frac{\partial \boldsymbol{F}_v}{\partial \eta} + \boldsymbol{S} \tag{9}$$

where $\boldsymbol{Q}$ is an unknown variable vector, $\boldsymbol{E}$, $\boldsymbol{F}$ are flux vectors and $\boldsymbol{E}_v$, $\boldsymbol{F}_v$ are viscous terms. $\boldsymbol{S}$ is the source term.

$$\boldsymbol{Q} = J\begin{pmatrix} \rho \\ \rho u \\ \rho v \\ e \\ \rho Y \end{pmatrix}, \quad \boldsymbol{E} = J\begin{pmatrix} \rho U \\ \rho u U + \xi_x p \\ \rho v U + \xi_y p \\ \rho U H \\ \rho U Y \end{pmatrix}, \quad \boldsymbol{F} = J\begin{pmatrix} \rho V \\ \rho u V + \eta_x p \\ \rho v V + \eta_y p \\ \rho V H \\ \rho V Y \end{pmatrix},$$

$$\boldsymbol{E}_v = J\begin{pmatrix} 0 \\ \xi_x \tau_{xx} + \xi_y \tau_{xy} \\ \xi_x \tau_{yx} + \xi_y \tau_{yy} \\ \xi_x T_{11} + \xi_y T_{22} \\ \xi_x \Re Y_x + \xi_y \Re Y_y \end{pmatrix}, \quad \boldsymbol{F}_v = J\begin{pmatrix} 0 \\ \eta_x \tau_{xx} + \eta_y \tau_{xy} \\ \eta_x \tau_{yx} + \eta_y \tau_{yy} \\ \eta_x T_{11} + \eta_y T_{22} \\ \eta_x \Re Y_x + \eta_y \Re Y_y \end{pmatrix}, \quad \boldsymbol{S} = J\begin{pmatrix} 0 \\ 0 \\ 0 \\ 0 \\ S_e - S_c \end{pmatrix}$$

where the Jacobian J of the transformation from Cartesian coordinates x_i to general curvilinear coordinates ξ_i is defined as $J \equiv \partial(x, y)/\partial(\xi, \eta) = x_\xi y_\eta - x_\eta y_\xi$. The relationships between the physical velocity u_i in x_i space and the contravariant velocity U_i in ξ_i space are $U_i = (\partial \xi_i / \partial x_j) u_j$ and $u_i = (\partial x_i / \partial \xi_j) U_j$ respectively, using the summation convention. $T_{11} = u\tau_{xx} + v\tau_{xy} + \kappa \partial T/\partial x$, $T_{22} = u\tau_{yx} + v\tau_{yy} + \kappa \partial T/\partial y$ and κ is the coefficient of thermal conductivity. Also, $\Re$ is the effective exchange coefficient, Se is the rate of evaporation and Sc is the rate of condensation.

The stress tensor τ, the mixture density ρ and the mixture viscosity μ [17] can be expressed as

$$\tau_{xx} = \frac{2}{3}\mu\left(2\frac{\partial u}{\partial x} - \frac{\partial v}{\partial y}\right), \quad \tau_{yy} = \frac{2}{3}\mu\left(2\frac{\partial v}{\partial y} - \frac{\partial u}{\partial x}\right),$$

$$\tau_{xy} = \tau_{yx} = \mu\left(\frac{\partial u}{\partial y} + \frac{\partial v}{\partial x}\right), \quad \rho = (1-\alpha)\rho_\ell + \alpha \rho_g,$$

$$\mu = (1-\alpha)(1+2.5\alpha)\mu_\ell + \alpha \mu_g.$$

H in Eq.(5) is the enthalpy defined by total energy $e = \rho H - p$.

4. Preconditioning Formulation

The hydraulic flow including cavitations can be characterized as fully three-dimensional, non-linear, viscous flow with laminar and turbulent regions. In addition, this flow with hydraulic transients and hydroacoustics has compressible flow characteristic at low Mach number. For such a flow, a compressible flow model that includes a preconditioning method [18,19] is advantageous. Preconditioning is a way to extend the functionality of existing codes for fully compressible flows to almost incompressible flows.

Applying the preconditioning method to Eq.(5), we obtain 2-D preconditioned governing equations with unknown variable vectors $\boldsymbol{W} = [p, u, v, T, Y]^T$ written in curvilinear coordinates as follows [13]:

$$\Gamma^{-1}\frac{\partial \boldsymbol{W}}{\partial \tau} + \Gamma_w^{-1}\frac{\partial \boldsymbol{W}}{\partial t} + \frac{\partial (\boldsymbol{E} - \boldsymbol{E}_v)}{\partial \xi} + \frac{\partial (\boldsymbol{F} - \boldsymbol{F}_v)}{\partial \eta} = \boldsymbol{S} \tag{10}$$

In this study, τ is pseudo-time and Γ_w^{-1} is a transform matrix of the Jacobian matrix $\partial \boldsymbol{Q}/\partial \boldsymbol{W}$. The preconditioning matrix Γ^{-1} is formed by the addition of the vector $\theta[1, u, v, H, Y]^T$ to the first column of the Γ_w^{-1} as,

$$\Gamma^{-1} = J \begin{pmatrix} \theta + \rho_p & 0 & 0 & \rho_T & \rho_Y \\ u\theta + u\rho_p & \rho & 0 & u\rho_T & u\rho_Y \\ v\theta + v\rho_p & 0 & \rho & v\rho_T & v\rho_Y \\ H\theta + H\rho_p - 1 & \rho u & \rho v & \rho C_p + H\rho_T & H\rho_Y \\ Y\theta + Y\rho_p & 0 & 0 & Y\rho_T & \rho + Y\rho_Y \end{pmatrix} \tag{11}$$

Parameter θ is chosen by Weiss & Smith [20],

$$\theta = \frac{1}{a^2} - \frac{1}{c^2}, \quad a^2 = \min[c^2, \max(|\boldsymbol{u}|^2, \beta|U_0|^2)] \tag{12}$$

where, U_0 is a fixed reference velocity such as average incoming freestream velocity, β is a constant which will be determined empirically for the appropriate precondition. In general, the value of β will be chosen so that θ becomes small because, if there is no problem with stability, small θ gives better solution for governing equation (9). In addition, time accuracy of the solution of Eq.(10) is independent of the pseudo-time term because when the pseudo-time integration converge, next physical time step is marched.

The source terms of the rate of evaporation and condensation in Eq.(9) can be assumed as functions of pressure and other selected parameters. For example, S_e for transformation of liquid to vapor and S_c for vapor to liquid are modeled as being proportional to the vapor mass fraction and pressure difference between the local pressure and vapor pressure (p_v) as,

$$Se = C_e(1 - Y)\max(0,\ p_v - p), \quad Sc = C_c Y \max(0,\ p - p_v) \tag{13}$$

where, C_e and C_c are empirical constants. These terms are similar to those used by Singhal et al. [3] and Kunz et al. [21] for both evaporation and condensation under the conditions that heat conduction and thermal effects on phase change are neglected.

5. Numerical Method

Fundamental equations (9) and (10) are solved by using appropriate numerical methods such as finite-difference method with TVD-MacCormack scheme [11] or TVD Runge-Kutta method [13]. For example, the preconditioned governing equations (10) are numerically integrated using the three-point backward finite-difference method of the dual time-stepping integration procedure. Then, Roe's flux difference splitting (FDS) method [22] with the MUSCL-TVD scheme [8] is applied to enhance the numerical stability, especially for steep gradients in density and pressure near the gas-liquid interface. Therefore, the derivative of the flux vector, for instance, $\boldsymbol{E}$ with respect to ξ at point i can be written with the numerical flux as $(\partial \boldsymbol{E}/\partial \xi) = (\boldsymbol{E}_{i+1/2} - \boldsymbol{E}_{i-1/2})/\Delta\xi$ and then, the approximate Riemann solver based on the Roe's FDS is applied. Hence, the numerical flux $\boldsymbol{E}_{i+1/2}$ is written as

$$\boldsymbol{E}_{i+1/2} = \frac{1}{2}\{\boldsymbol{E}(\boldsymbol{Q}^L_{i+1/2}) + \boldsymbol{E}(\boldsymbol{Q}^R_{i+1/2}) - Z^{-1}_{i+1/2}(\boldsymbol{L_p}^{-1}|\Lambda|\boldsymbol{L_p})_{i+1/2}(\boldsymbol{W}^R_{i+1/2} - \boldsymbol{W}^L_{i+1/2})\} \tag{14}$$

where, Λ is the diagonal matrix of eigenvalues and $\boldsymbol{L_p}$ and $\boldsymbol{L_p}^{-1}$ are the left eigenvectors of $Z\partial \boldsymbol{E}/\partial \boldsymbol{W}$. $Z^{-1} = \Gamma^{-1} + \Gamma_w^{-1}\delta 3/2$, $\delta = \Delta\tau/\Delta t$, $\tilde{U} \pm \tilde{c} = U/\alpha - (B \mp \sqrt{B^2 + 4Ac^2 g_{11}/\alpha})/2$, and

$$\Lambda = \begin{pmatrix} \tilde{U} & & & & 0 \\ & \tilde{U} + \tilde{c} & & & \\ & & \tilde{U} & & \\ & & & \tilde{U} - \tilde{c} & \\ 0 & & & & \tilde{U} \end{pmatrix}, \quad \boldsymbol{L_p} = \begin{pmatrix} 1 & 0 & 0 & -\rho C_p & 0 \\ 1 & \xi_x \ell^- & \xi_y \ell^- & 0 & 0 \\ 0 & \xi_y & -\xi_x & 0 & 0 \\ 1 & \xi_x \ell^+ & \xi_y \ell^+ & 0 & 0 \\ 0 & -\xi_y & \xi_x & 0 & 1 \end{pmatrix}$$

$$\ell^{\pm} = \frac{-2\rho c^2 A}{B \pm \sqrt{B^2 + 4Ac^2 g_{11}/\alpha}}, \quad A = \frac{\rho_T + \rho C_p \rho_p}{\rho_T \alpha + \rho C_p(\theta + \rho_p \alpha)}, \quad B = \frac{U/\alpha \rho C_p \theta}{\rho_T \alpha + \rho C_p(\theta + \rho_p \alpha)}$$

where $\alpha = 1 + \delta 3/2$, $\rho_p = \partial\rho/\partial p$, $\rho_T = \partial\rho/\partial T$, $g_{11} = \xi_x^2 + \xi_y^2$, and the eigenvectors are estimated by introducing Roe's averaging. $\boldsymbol{W}_{i+1/2}^{L,R}$ is obtained by applying the third-order MUSCL-TVD scheme as

$$\begin{aligned}
\boldsymbol{W}_{i+1/2}^{L} &= \boldsymbol{W}_i + (\phi/4)\{(1-\kappa)D^+\boldsymbol{W}_{i-1/2} + (1+\kappa)D^-\boldsymbol{W}_{i+1/2}\} \\
\boldsymbol{W}_{i+1/2}^{R} &= \boldsymbol{W}_{i+1} - (\phi/4)\{(1-\kappa)D^-\boldsymbol{W}_{i+3/2} + (1+\kappa)D^+\boldsymbol{W}_{i+1/2}\}
\end{aligned} \tag{15}$$

Here, the flux-limited values of $D\boldsymbol{W}$ and the minmod function are determined by

$$\begin{aligned}
&D^+\boldsymbol{W}_{i-1/2} = \mathrm{minmod}(\delta\boldsymbol{W}_{i-1/2}, b\delta\boldsymbol{W}_{i+1/2}), \\
&D^-\boldsymbol{W}_{i+1/2} = \mathrm{minmod}(\delta\boldsymbol{W}_{i+1/2}, b\delta\boldsymbol{W}_{i-1/2}), \\
&\delta\boldsymbol{W}_{i+1/2} = \boldsymbol{W}_{i+1} - \boldsymbol{W}_i, \\
&\mathrm{minmod}(x, y) = \mathrm{sign}(x)\max[0, \min\{|x|, y\mathrm{sign}(x)\}]
\end{aligned} \tag{16}$$

The linear combination parameter κ is determined by the range of $-1 \le \kappa \le 1$ and has an effect on the accuracy. That is, Eq.(14) has 3rd-order accuracy at $\kappa = 1/3$ and ϕ=1. At ϕ=0, this equation has first-order accuracy [23]. Typically, flows with cavitation contain regions with sharp interfaces between liquid and gas phases. However, application of the 3rd-order upwind bias scheme to these regions gives over- or undershoots for the solution at these interfaces, which can be a cause of the instability in the computation, particularly for the mass fraction equations. In order to improve this difficulty, the flux evaluation is made locally first-order in the presence of sharp gradients in the mixture quality Y. This is achieved through the application of an artificial dissipation such as a second-order dissipations by Jameson et al. [24]. Specifically, a dissipation is expressed for each coordinate direction as $\phi_i = 1 - d_i$ in Eq.(15). The term of artificial dissipation d_i is defined as $d_i = |Y_{i+1} - 2Y_i + Y_{i-1}|/(Y_{i+1} + 2Y_i + Y_{i-1})$, and is very small except in the immediate vicinity of gas-liquid interfaces. On the other hand, the slope of the flux in the minmod function is controlled by the limiter b. The range of b, $1 \le b \le (3-\kappa)/(1-\kappa)$, is determined by the condition of TVD stablility. In this computation, a b of 4 and a κ of 1/3 are used. Numerical damping arisen from TVD upwing scheme probably affects the accuracy. In the previous investigation [23], however, it was confirmed that the effect of the damping was limited and there was no sharp drop in accuracy.

In the numerical integration of governing equations (10), the third-order TVD Runge-Kutta explicit method written followings is used.

$$\boldsymbol{W}^{(1)} = \boldsymbol{W}^n - \Delta t \Gamma \boldsymbol{L}(\boldsymbol{Q}^n) \tag{17}$$

$$\boldsymbol{W}^{(2)} = \frac{3}{4}\boldsymbol{W}^n + \frac{1}{4}\{\boldsymbol{W}^{(1)} - \Delta t \Gamma \boldsymbol{L}(\boldsymbol{Q}^{(1)})\} \tag{18}$$

$$\boldsymbol{W}^{n+1} = \frac{1}{3}\boldsymbol{W}^n + \frac{2}{3}\{\boldsymbol{W}^{(2)} - \Delta t \Gamma \boldsymbol{L}(\boldsymbol{Q}^{(2)})\} \tag{19}$$

where,

$$\boldsymbol{L}(\boldsymbol{Q}) = \frac{\partial(\boldsymbol{E} - \boldsymbol{E}_v)}{\partial\xi} + \frac{\partial(\boldsymbol{F} - \boldsymbol{F}_v)}{\partial\eta} - \boldsymbol{S}$$

6. Numerical Results

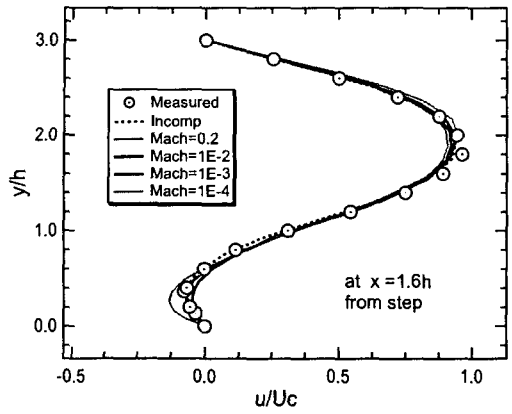

Fig.1 Comparison of velocity profiles for a backward-facing step at several Mach numbers

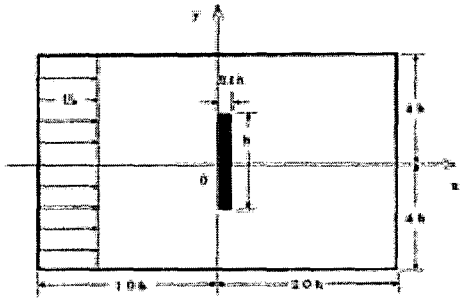

Fig.2 Computational domain and coordinate system

At first, the present computational method is validated with the noncavity laminar duct flow over a backward-facing step which is often used as the benchmark problem to check the numerical algorithm. In this computation, the expansion ratio of the duct is 1.5 which is the same as the geometry studied experimentally by Kueny and Binder [25]. The Reynolds number Re is 150 based on the step height h and inlet maximum velocity Uc. A body-fitted curvilinear coordinates grid with 90×21 grid points is used.

Figure 1 shows comparisons of streamwise velocities at the downstream location of x/h=1.6 behind the step with experimental data. In the computation for steady state laminar single-phase flow at several inlet Mach number, β of 0.1 in Eq.(12) was used except the case of inlet Mach number of $M_{in} = 0.2$ computed without preconditioning. The results obtained by present preconditioning method are fairly well predicted. It seems that differences between experimental data are increased with decrement of the Mach number, because of increment of θ in Eq.(12) for constant β of 0.1. The difference can be controled by choosing appropriate β. It is confirmed that at nearly incompressible flow condition with inlet Mach number of 1×10^{-4}, the present method still maintaines and shows a reasonable solution. In addition, we know that the flow at $M_{in} = 0.2$ is solved by the present compressible flow formulation of Eq.(9) without θ and predicted well.

As reference, results by obtained using the incompressible Navier-Stokes solver by Shin et al. [26] are also shown in this figure. The separated region, the following reattachment and the typical channel flow pattern after recovery from the recirculating flow are clearly observed.

Next, with the validation investigated above, an external cavity flow around a flat plate normal to flow is calculated at some different cavitation numbers from subcavitation state to

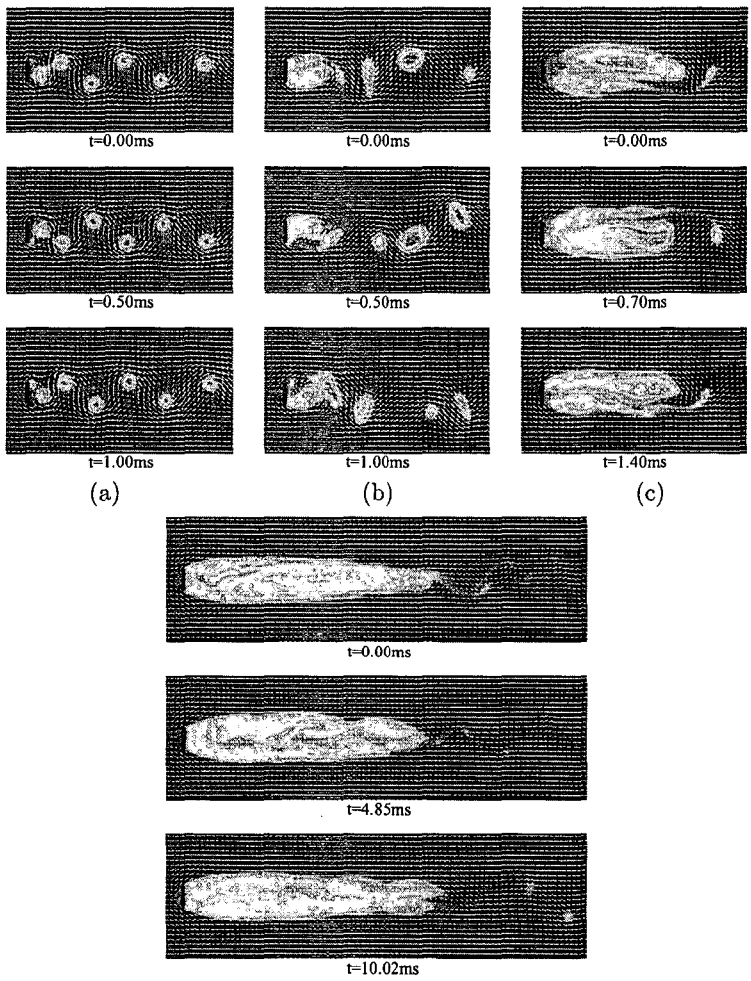

Fig.3 Time evolution of void fraction contours and velocity vectors for (a) σ=4.35, (b) σ=2.44, (c) σ=1.68 and (d) σ=1.18

supercavitation state. The up- and downstream boundaries of the computational domain are located at distances $10h$ up and $20h$ downstream from the plate, which has height h and thickness of $0.1h$ in Fig.2. The upper and lower boundaries are located $4h$ from either side of the plate center. A total number of 1501×401 equispaced grid points are used. The cavitation number σ is defined by $\sigma = (p_0 - p_v)/(0.5\rho_0 u_0^2)$, where p_v represents the vapor pressure and subscript "0" means the value at the upstream point. The cavity flow conditions for calculation are $Re_0 = 9 \times 10^3$, $\alpha_0 = 0.001$, and σ=4.35, 2.44, 1.68 and 1.18.

Figures 3(a)-(d) show time evolutions of instantaneous void fraction as well as velocity vectors of the flow around a flat plate. In Fig.3(a), for $\sigma = 4.35$, there is no observable cavitation attached to the rear surface, while a Karman vortex grows and sheds alternately from either corners of the plate. The void fraction α is high in the center of the vortex, so that the vortex cavitation is formed. At $\sigma = 2.44$ in Fig.3(b), the fixed cavitation appears and the cavity length and width is fluctuated dynamically with time behind the plate where the pressure is very close to the vapor pressure. Beyond $2h$ downstream from the plate, the vortex cavitation,

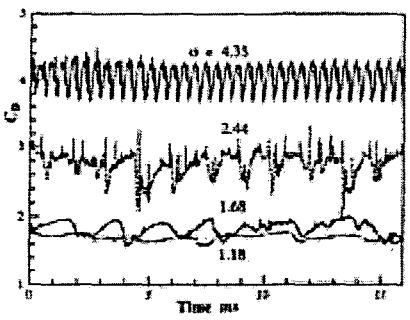

Fig.4 Time evolution of drag coefficient

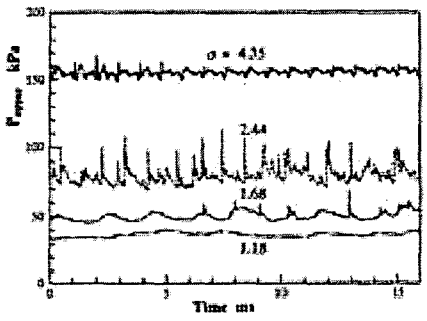

Fig.5 Time evolution of drag coefficient

which is formed by shedding from the fixed cavitation, makes an another kind of vortex street indicating the transitional cavity flow phenomena. From Figs.3(c) and (d) for $\sigma = 1.68$ and 1.18, both the cavity length and width increase with decreasing σ, and the period of vortex shedding from the cavity also becomes longer. It can also be seen that the appearance of the re-entrant jet and the void distribution inside the cavity is much more complicated than in Fig.3(a) or (b). The cavitation pattern in Fig.3(d) is close to the supercavitation state and exhibits weak unsteadiness.

Figures 4 and 5 show respectively time evolutions of drag coefficient and pressure p_{upper} monitored at a $3h$ upper position from the plate for each cavitation number. It is indicated that the fluctuations of both drag and pressure are the most irregular at $\sigma = 2.44$ in the typical transition region, and their amplitudes decrease little by little at the low cavitation number. The exponential fluctuations also tend to suggest the generation of many shock waves due to the rapid cavity volume changes. These shock waves propagate through the flow fields. The present method is therefore suitable for capturing shock wave-based phenomena, which is an important cavity flow characteristics, because the method takes account of the compressibility of gas-liquid two-phase media.

7. Conclusions

A high resolution scheme developed by the author for analysing gas-liquid two-phase flows with cavitation was introduced. The fundamental equations of these schemes are the density based momentum equations for mixture of gas-liquid medium in the curvilinear coordinates. A cavitation model based on a homogenous equilibrium model of gas-liquid two-phase media was employed to solve cavitating flows. These schemes have been extended to preconditioning method to treat both compressibility and incompressibility effects associated with very large range of mixture sound speeds.

Computed results for the cavity flow pattern behind the flat plate were compared with analytic results and experimental data, and they agree fairly well with each other. Some detailed observations of void fraction, velocity and pressure distributions were presented. From the unsteady results of the void fraction and velocity field in the cavity, the complex cavity flow behaviors of the cavitation occurrence and its growing and shedding were clarified. It was confirmed that the present method with a homogenous cavitation model gave us good computational performance and reliability even at the low Mach number flow.

Acknowledgment

The authors would like to acknowledge the support from KISTI (Korea Institute of Science and Technology Information) under 'The Sixth Strategic Supercomputing Support Program.'

The use of the computing system of the Supercomputing Center is also greatly appreciated.

References

[1] Reboud, J.L. and Stutz, B., "Two-Phase Flow Structure of Cavitation: Experimental and Modeling of Unsteady Effects," *Proc. 3rd Int. Symp. on Cavitation*, Vol.1, (1998), pp.203-208.

[2] Chen, Y., and Heister, S.D., "Two-Phase Modeling of Cavitated Flows," *Computers & Fluids*, Vol.24, (1995), pp.799-809.

[3] Singhal, A.K., Vaidya, N. and Leonard, A.D., "Multi-Dimensional Simulation of Cavitating Flows Using a PDF Model for Phase Change," *ASME Paper* FEDSM97-3272, (1997).

[4] Merkle, C.L., Feng, J.Z. and Buelow, P.E.O., "Computational Modeling of the Dynamics of Sheet Cavitation," *Proc. 3rd Int. Symp. on Cavitation*, Vol.2, (1998), pp.307-311.

[5] Shin, B.R., Iwata, Y. and Ikohagi, T., "Numerical Simulation of Unsteady Cavitating Flows Using a Homogeneous Equilibrium Model," Computational Mechanics, Vol.30, No.5-6, (2003), pp.388-395.

[6] Shin, B.R., and Ikohagi, T., "Numerical Analysis of Unsteady Cavity Flows around a Hydrofoil," *ASME Paper* FEDSM99-7215, (1999).

[7] Yee, H.C., "Upwind and Symmetric Shock-Capturing Scheme," NASA TM-89464, (1987).

[8] van Leer, B., "Towards the Ultimate Conservative Difference Scheme V. A Second-Order Sequel to Godunov's Method," *J. Comp. Phys.*, Vol.32, (1979), pp.101-136.

[9] Shin, B.R., "Numerical Analysis of Unsteady Cavitating Flow by a Homogeneous Equilibrium Model," *AIAA Paper* 2001-2909, (2001).

[10] Iga, Y., Nohmi, M., Goto, A., Shin, B.R. and Ikohagi, T., "Numerical Analysis of 2-D Unsteady Cavitating Flow Around Hydrofoils in Cascade," *Trans. JSME*, Ser. B, Vol.68, No.666 (2002), pp.78-84.

[11] Iga, Y., Nohmi, M., Goto, A., Shin, B.R. and Ikohagi, T., "Numerical Study of Cavitation Break-off Phenomenon on Hydrofoils," *ASME J. Fluid Engng.*, Vol.125, No.4 (2003), pp.643-651.

[12] Shin, B.R., Iga, Y. and Ikohagi, T., "Numerical Analysis of Cavitating Flow through a 2-D Decelerating Cascade," *Computational Fluid Dynamics 2000*, (ed., N. Satofuka), Springer-Verlag, Berlin (2001), pp.651-656.

[13] Shin, B.R., Yamamoto, S. and Yuan X., "Application of Preconditioning Method to Gas-Liquid Two-Phase Flow Computations," *ASME J. Fluid Engng.*, Vol.126, No.4 (2004), pp.605-612.

[14] Shin, B.R. and Yamamoto, S., "A Preconditioning Method for Two-Phase Flows with Cavitation," *Comp. Fluid Dyn. J.*, Vol.13, No.4 (2005), pp.722-729.

[15] Chen, H.T., and Collins, R., "Shock Wave Propagation Past on Ocean Surface," *J. Comp. Phys.*, Vol.7, (1971), pp.89-101.

[16] Karplus, H.B., ARF-4132-12, (1961) or Akagawa, K., Gas-Liquid Two-Phase Flow, Corona Pub., Tokyo (1974), pp.226-246.

[17] Beattie, D.R.H., and Whally, P.B., "A Simple Two-Phase Frictional Pressure Drop Calculation Method," *Int. J. Multiphase Flow*, Vol.8, (1982), pp.83-87.

[18] Turkel, E., "Preconditioning Methods for Solving the Incompressible and Low Speed Compressible Equations," *J. Comput. Phys.*, Vol.72, (1987), pp.277-298.

[19] Venkateswaran, S. and Merkle, C.L., "Analysis of Preconditioning Method for the Euler and Navier-Stokes Equations," *Von Karman Institute Lecture Series*, 1999-03, (1999).

[20] Weiss, J.M., and Smith, W.A., "Preconditioning Applied to Variable and Constant Density Flows," *AIAA J.*, Vol.33, (1995), pp.2050-2057.

[21] Kunz, R.F. et al., "A Preconditioned Navier-Stokes Method for Two-Phase Flows with Application to Cavitation Prediction," *Computers & Fluids*, Vol.29, (2000), pp.849-875.

[22] Roe, P.L., "Approximate Riemann Solvers, Parameter Vectors and Difference Scheme," *J. Comp. Phys.*, Vol.43, (1981), pp.357-372.

[23] Shin, B.R., "A Stable Numerical Method Applying a TVD Scheme for Incompressible Flow," *AIAA J.*, Vol.41, No.1, (2003), pp.49-55.

[24] Jameson, A., et al., "Numerical Solutions of the Euler Equations by Finite Volume Methods using Runge-Kutta Time-Stepping Schemes," *AIAA paper* 81-1259, (1981).

[25] Kueny, J.L., and Binder, G., "Viscous Flow over Backward Facing Steps, An Experimental Investigation," *Note on Numerical Fluid Mechanics*, Vol.9, Vieweg, (1984), pp.32-47.

[26] Shin, B.R., Ikohagi, T. and Hisaaki, D., "An Unsteady Implicit SMAC Scheme for Two-Dimensional Incompressible Navier-Stokes Equations," *JSME Int, J.*, Vol.36-B, (1993), pp.598-606.